Showcasing research from Dr Miguel Monge's laboratory, Department of Chemistry, University of La Rioja, Spain.

Single-step assembly of gold nanoparticles into plasmonic colloidosomes at the interface of oleic acid nanodroplets

Gold colloidosomes (Au CSs) are obtained in a single step procedure by the decomposition of an organometallic Au(I) precursor at the interface of oleic acid nanodroplets in *n*-hexane. Oleic acid performs a multiple role as template, reactant and stabilizing agent for the self-assembled colloidosomes. A precise control over the size, the shape and the surface of the obtained Au CSs is exerted and, therefore, the tuning of their collective plasmonic properties is achieved. The white-light induced photothermal heating of these systems and their stimuli-responsive properties upon solvent or glutathione addition are studied.

As featured in:

See Miguel Monge *et al.*,
Nanoscale Adv., 2021, **3**, 198.

ROYAL SOCIETY OF CHEMISTRY

rsc.li/nanoscale-advances

PAPER

Check for updates

Single-step assembly of gold nanoparticles into plasmonic colloidosomes at the interface of oleic acid nanodroplets†

José M. López-de-Luzuriaga, [iD] Miguel Monge, [iD] * Javier Quintana [iD] and María Rodríguez-Castillo [iD]

Plasmonic gold colloidosomes (Au CSs) of sub-200 nm size are formed by the self-assembly of spherical gold nanoparticles (Au NPs) of *ca.* 4 nm size at the interface of oleic acid (OA) nanodroplets formed in *n*-hexane. Au NPs are prepared through the mild decomposition of [Au(C$_6$F$_5$)(tht)] (tht = tetrahydrothiophene). These Au CSs display tunable surface, size and shape-dependent collective plasmonic absorptions, leading to interesting photothermal and stimuli-responsive properties.

Introduction

The self-assembly of nanoparticles constitutes a robust approach for the construction and application of precisely controlled complex nanostructures displaying superior collective properties.[1] In addition, and taking into account a possible dynamic nature, a very important characteristic of some of these nanosystems is their ability to disassemble/reassemble *via* external stimuli like temperature, pH, metal ions, (bio) molecules or solvent composition, leading to promising smart nanomaterials.[2,3]

Colloidosomes (CSs), which consist of 3D porous and hollow nano- or microcapsules with closed-packed colloidal nanoparticles at their surface, are an interesting class of these self-assembled nanostructures.[4,5] These CSs display attractive properties such as the encapsulation of drugs or proteins for drug delivery or controlled release, with potential applications in imaging, biomedicine and biosensing.[6,7]

Plasmonic gold colloidosomes (Au CSs)[8–12] have recently emerged as a promising class of assembled nanostructures since, in addition to the above mentioned properties, new ones related to their collective plasmonic nature, such as improved solar energy harvesting and photothermal heating, remarkable SERS activity and catalytic or photocatalytic applications have been recently reported.

Synthetic approaches for Au CSs of different sizes include, for instance, the electrostatic self-assembly of Au NPs on silica nanosphere templates;[8] emulsions at the oil–water interface;[9,11]

growth of Au NPs onto dendritic fibrous silica,[10] or a reverse (water-in-1-butanol) emulsion system.[12] Most of these synthetic approaches require several steps to achieve Au CSs. The development of new synthetic approaches for the synthesis of nanoscale colloidosomes with high size monodispersity will provide unique collective properties. At this regard, the preparation of nano-sized Au CSs is highly challenging due to the reduced Helmholtz free energy for small-size (much less than 50 nm) nanoparticles at liquid–liquid interfaces.[11]

Very interestingly, a recent result by Sciortino *et al.* have dealt with the possibility of formation of solvent nanodroplets of *ca.* 100 nm in macroscopically miscible mixtures of water and tetrahydrofuran, which serve as templates for the formation of polymer-nanoparticle hybrid nanocapsules so-called hybridosomes.[13,14]

On the other hand, we have devoted a part of our research efforts to the preparation of well-controlled plasmonic Au and/ or Ag nanostructures by the mild decomposition of pentafluorophenyl-based gold(I) and/or silver(I) precursors.[15–17] In one of these studies we focused on the key role played by oleic acid (OA) when it was used as precursor, reactant, solvent and capping agent at the same time, in the formation of plasmonic ultrathin gold–silver nanorods and nanowires from the organometallic precursor [Au$_2$Ag$_2$(C$_6$F$_5$)$_4$(OEt$_2$)$_2$]$_n$.[18] The very nice control exerted by OA to the plasmonic nanostructures prompted us to continue our studies in this direction. At this point we have wondered whether OA would react with the pentafluorophenyl ligand in complex [Au(C$_6$F$_5$)(tht)] (tht = tetrahydrothiophene) leading to a mild decomposition of this complex and, consequently, to the formation of new well-controlled gold nanostructures with interesting plasmonic properties. In this work we report a novel single-step approach for the synthesis of nano-sized plasmonic Au CSs formed by the self-assembly of small and monodisperse Au NPs (*ca.* 4 nm diameter) (see Scheme 1). This self-assembly takes place at the

Departamento de Química, Universidad de La Rioja, Centro de Investigación en Síntesis Química (CISQ), Complejo Científico-Tecnológico, 26006-Logroño, Spain. E-mail: miguel.monge@unirioja.es
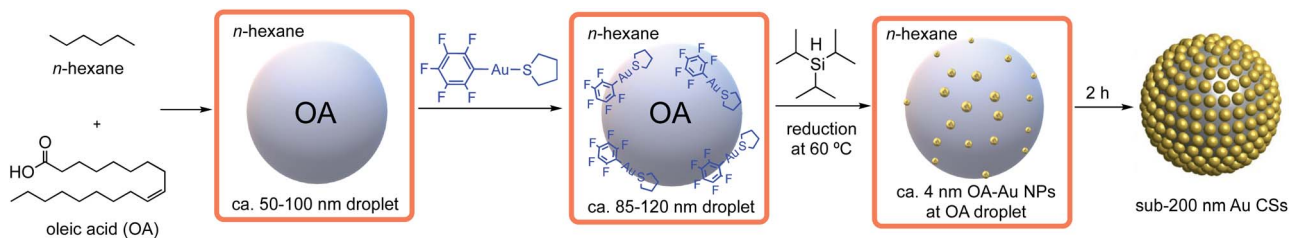
Scheme 1 Synthesis of Au CSs at the interface of oleic acid nanodroplet templates.

liquid–liquid interface of OA nanodroplets of *ca.* 50–100 nm in *n*-hexane, which are macroscopically miscible liquids. To the best of our knowledge this type of fatty acid nanodroplets formed in an organic solvent has not been reported. As in our previous studies, OA plays a key and multiple role, since it provides a nanodroplet template with an active interface for the Au CSs formation. In addition, OA acts as reactant towards $C_6F_5^-$ abstraction from the Au(I) precursor and as capping ligand for the formed Au NPs at this interface. We also report on the surface, size and shape-dependent collective plasmonic properties of these Au CSs; their white-light induced photo-thermal heating and on stimuli-responsive properties of these nanosystems such as solvent change or glutathione (GSH) addition. In addition, when using GSH, Au CSs can be isolated from the OA, while remaining their morphology almost unaltered and allowing their solubility in water, boosting their potential use in different fields.

Results and discussion

Synthesis, morphology and plasmonic properties of Au CSs

Decomposition of complex $[Au(C_6F_5)(tht)]$ (8.8 mM) was carried out in *n*-hexane (2.5 mL) as solvent, in the presence of OA (0.128 M) and the reducing agent triisopropylsilane TIPS (0.292 M) (see ESI for details†). After 2 h of reaction a deep blue solution of Au CSs (**1**) of 179 ± 29 nm size (observed in the Transmission Electron Microscopy (TEM) micrographs (Fig. 1A and B)) were spontaneously obtained in a single step. In Fig. 1C and D, we present the TEM micrographs of Au CSs (**2**) and (**3**) with a diameter of 139 ± 23 nm (**2**) and 185 ± 23 nm (**3**). Au CSs **2** and **3** were obtained through the decomposition of lower, 4.4 mM (**2**), or higher, 13.2 mM (**3**), amounts of $[Au(C_6F_5)(tht)]$, respectively, and in the presence of a fixed OA concentration of 0.128 M. The results show the formation of more compact colloidosomes, in the case of Au CSs (**2**), and spherical colloidosomes with large hollow cavities, in the case of Au CSs (**3**), as for Au CSs (**1**). In the case of **2** it seems that the small size of the individual Au NPs formed at the liquid–liquid interface and the larger OA ratio lead to the formation of thicker shells of packed Au NPs. In all cases, the Au CSs were formed through the self-assembly of spherical Au NPs of *ca.* 3–4 nm size (see size histograms in ESI). Also, using different OA concentrations with a fixed Au(I) precursor concentration of 8.8 mM, Au CSs (**4**) and (**5**) were also obtained (Fig. 2A and B). In this case, the addition of a lower OA concentration (0.064 M) allowed the synthesis of

urchin-like Au CSs (**4**) of 192 ± 32 nm size (nanoparticles of 3.3 ± 1.1 nm size) with short nanorods at their surface. On the other hand, when a larger amount of OA was used (0.38 M), highly dense Au CSs (**5**) of 173 ± 27 nm size (nanoparticles of 2.9 ± 0.7 nm size) with thick shells of packed Au NPs of small size, similar to Au CSs (**2**), were obtained.

We also checked the influence of adding a higher amount of TIPS (0.88 M) to the reaction mixture used for the synthesis of Au CSs (**1**), leading to very similar Au CSs (**6**) of 189 ± 31 nm size (ESI†).
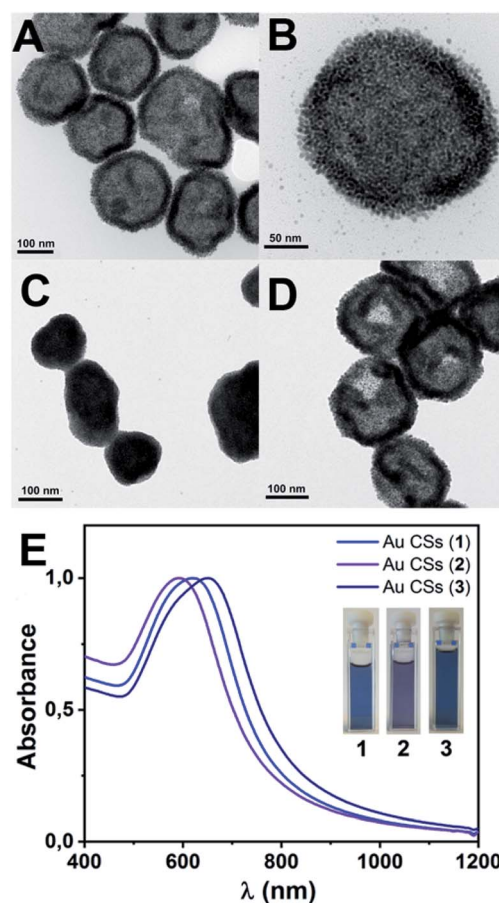

Fig. 1 (Top) TEM images of Au CSs obtained with different Au(I) precursor concentrations: 8.8 mM for Au CSs (**1**) (A and B); 4.4 mM for Au CSs (**2**) (C) or 13.2 mM for Au CSs (**3**) (D). (Bottom) Normalized UV/Vis spectra of Au CSs **1–3** in *n*-hexane (E).
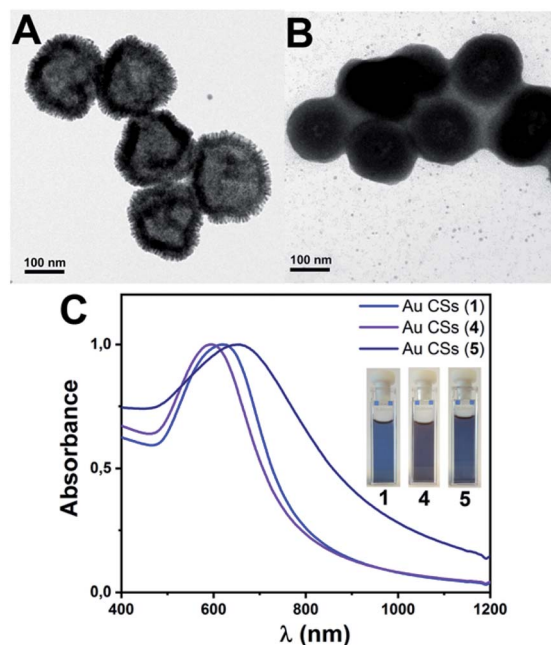
Fig. 2 (Top) TEM images of Au CSs obtained with different amounts of OA keeping 8.8 mM for the Au(I) precursor: 0.064 M for Au CSs (**4**) (A) or 0.38 M for Au CSs (**5**) (B). (Bottom) Normalized UV/Vis spectra of Au CSs **1**, **4** and **5** in *n*-hexane (C).

The plasmonic properties of the Au CSs are different to those of the individual Au NPs used as building blocks. This difference arises from the coupling of the individual NP plasmons due to the decrease of the interparticle distances. In addition, as it has been reported[19–21] for Au nanoshells, the hollow nature of these nanostructures is another key parameter for red-shift of the plasmonic absorption compared to the isolated Au NPs. The effect of this plasmonic coupling consists of more or less pronounced wavelength absorption red-shift and band broadening that depends on the size, the shape, the interparticle distance and the hollow cavity size of the obtained nanostructures.[22–24] We observe the tuning of these collective plasmonic properties for Au CSs **1–3** with a red-shift of the plasmonic absorption when increasing the diameter from 592 (**2**) to 622 (**1**) and to 650 nm (**3**) (Fig. 1E). Similarly, the surface shape control of the Au CSs leads to a blue-shifted absorption for the urchin-like Au CSs (**4**) at 595 nm and a red-shift absorption for the densely aggregated Au CSs (**5**) at 657 nm (Fig. 2C) with respect to Au CSs (**1**), respectively. Also, although the interparticle distance is not easy to measure in the obtained Au CSs we observe that the CSs showing a compact shape with smaller hollow cavities and with obviously shorter interparticle distance, show a more pronounced red-shift and broadening of the plasmonic absorption. Thus, Au CSs (**3**) display a thicker surface than that of Au CSs (**1**) and a concomitant red-shift of the plasmon absorption. Similarly, Au CSs (**5**) show a densely packed Au NPs and a slightly larger size to that of Au CSs (**1**), leading to an even more pronounced red-shift.

In addition, the plasmonic absorption of Au CSs (**1**) in different solvents such as *n*-hexane (614 nm), toluene (628 nm)

and ethanol (624 nm) appear slightly shifted due to the different refractive index of the solvents (see ESI†). The similar low-energy absorption wavelength (614–628 nm) displayed for the three solvents confirms the stability of the Au CSs in them.

In order to prove the hollow nature of the Au CSs and the different types of hollow cavities that could be obtained by changing the reaction parameters, we recorded energy-dispersive X-ray (EDX) spectra and line-scan intensity and elemental (gold) profiles, together with high angle annular dark field-scanning transmission electron microscopy (HAADF-STEM) images for Au CSs (**1**) and (**5**). Fig. 3A shows the HAADF-STEM image of a single colloidosome of sample Au CSs (**1**), showing a large hollow cavity. The line scan intensity profile displays the hollow nature of Au CSs (**1**) (Fig. 3B).

The corresponding EDX spectrum (Fig. 3C) shows the presence of gold, whereas the line-scan elemental profile (Fig. 3D) confirms the hollow nature, the thin shell thickness and the large cavity size of these nanostructures. In contrast, the HAADF-STEM (Fig. 3E) image and the line scan intensity (Fig. 3F) and elemental profiles (Fig. 3H) confirm that Au CSs (**5**) display a thicker shell and a smaller hollow cavity.

Finally, we have analysed the role of the Au complex : OA ratio in the final size and morphology of the obtained Au CSs (see ESI†). From this analysis it can be observed that for Au CSs (**1**) (1 : 14.5 Au complex : OA ratio), Au CSs (**3**) (1 : 9.7 Au complex : OA ratio) and Au CSs (**4**) (1 : 7.3 Au complex : OA ratio) a similar morphology of CSs with large hollow cavities is obtained. What it can be observed for these CSs is that decreasing the Au complex : OA ratio, the size of the Au CSs increases from 179 nm (**1**) to 192 nm (**4**). This trend would be related to a higher degree of interaction of OA with the CSs surface when a higher ratio of OA is added (**1**), precluding the growth to a larger size. On the other hand, in the case of Au CSs (**2**) (1 : 29.0 Au complex : OA ratio) and Au CSs (**5**) (1 : 43.2 Au complex : OA ratio) the OA ratio is much higher. This higher OA ratio seems to affect to the growth of the individual NPs (*ca.* 3 nm) and to their packing at the interface of the OA nanodroplets, leading to Au CSs with thicker shells and smaller hollow cavities.

Mechanism of formation of Au CSs

We hypothesized that OA was playing a key role in the formation of these Au CSs in a single-step through nanodroplet evolution and Pickering emulsion-like formation.

Indeed, following the observations of Sciortino *et al.*[13,14] for water/THF mixtures, we performed Nanoparticle Tracking Analysis (NTA) measurements (see Fig. 4). This technique permits the multiparameter analysis of Au CSs suspensions such as size, concentration and direct real-time observation. Briefly, a laser illuminates the Au CSs suspension in a sample holder and the Brownian motion of particles is analysed in real-time by a CCD camera by tracking the light scattering centres of the Au CSs and each particle is simultaneously but individually visualised and tracked, as it is observed in the optical microscopy images. The hydrodynamic diameter of each Au CS can be estimated through the Stoke–Einstein equation. In contrast to conventional methodologies of particle sizing, NTA is not
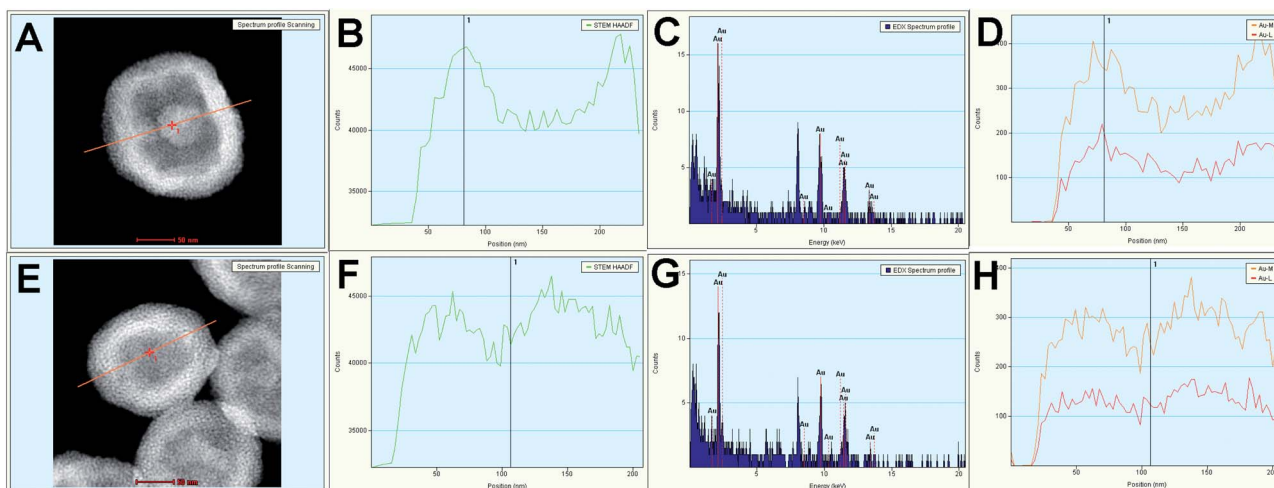
Fig. 3 HAADF–STEM image (A): HAADF line-scan intensity profile (B); energy-dispersive X-ray (EDX) spectra (C) and line-scan elemental gold profiles (D) for Au CSs **1**. HAADF–STEM image (E): HAADF line-scan intensity profile (F); energy-dispersive X-ray (EDX) spectra (G) and line-scan elemental gold profiles (H) for Au CSs **5**.
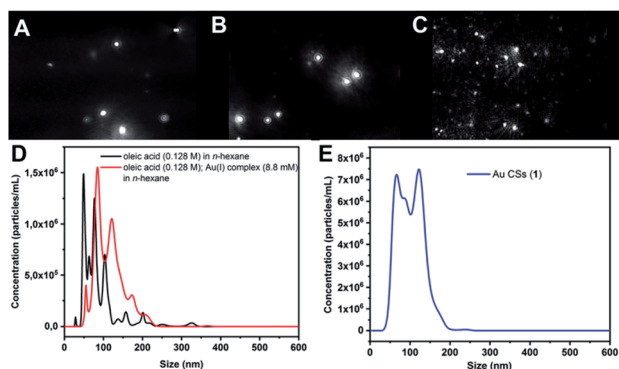

Fig. 4 Optical microscopy image of the scattered spotlights of an oleic acid/n-hexane mixture (A), Au(I) complex/oleic acid/n-hexane mixture (B) and Au CSs (**1**) (C). NTA analysis of an oleic acid/n-hexane mixture (black) and a Au(I) complex/oleic acid/n-hexane mixture (red) (D), NTA analysis of Au CSs (**1**) (blue) (E).

intensity weighted since each Au CS is tracked separately. The obtained results are provided as a size distribution and particle concentration together with optical microscopy images of the scattered spotlight. We studied first the behaviour of OA in n-hexane in similar conditions to those used in the formation of Au CSs (**1**). We observed the existence of droplets with hydrodynamic diameter D_h between 49–100 nm (mean: 90 nm; mode: 49 nm; st. dev.: 50 nm).

The NTA analysis of the reaction mixture, formed by the Au(I) precursor (8.8 mM) and OA (0.128 M) and n-hexane as solvent, showed nanodroplets of slightly larger D_h between 85–122 nm (mean: 116 nm; mode: 87 nm; st. dev.: 37 nm), showing a possible effect of interaction of the organometallic complex at the interface of the droplet template, since nanodroplet size increases. The existence of such organometallic-oleic acid droplets was confirmed through the TEM analysis that shows spherical particles of low contrast and between *ca.* 95–120 nm

size (Fig. 5), which could be related to these molecular intermediates. In addition, the analysis of the TEM micrograph shows the spontaneous formation of Au NPs at the surface of these low-contrast spherical particles, which corresponds in solution to the liquid–liquid interface (inset in Fig. 5).

Finally, the NTA analysis of Au CSs (**1**) showed up a population of scattering nano-objects of D_h between 214–600 nm (mean: 465 nm; mode: 465 nm; st. dev.: 114 nm). This result would be in agreement with the observation of agglomeration of colloidosomes as observed in the TEM image on Fig. 1A. The analysis of a diluted solution of Au CSs **1** shows a D_h between 67–123 nm (mean: 102 nm; mode: 122 nm; st. dev.: 32 nm) (see Fig. 4E), a value close to the size measurements through the analysis of the TEM micrographs. The larger diameter value observed for the TEM images would be related to the drying process of the grid samples and/or to the dynamic nature of the Au CSs in the diluted samples.

From a spectroscopic point of view we have performed ^{1}H, ^{13}C{^{1}H} and ^{19}F NMR and MS-ESI(−) studies in solution and IR
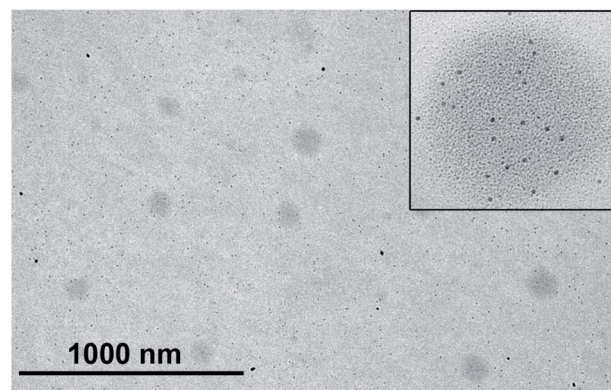

Fig. 5 TEM image of the Au(I) complex/oleic acid/n-hexane mixture. The inset shows an image from the same sample showing the initial formation of Au NPs at the surface of the nanodroplets.

spectroscopy in solid state in order to elucidate the mechanism of formation of the Au CSs and the role played by OA (see ESI†). Apart from the possibility of formation of a $[Au(C_6F_5)(OA)]$ intermediate and the deprotonation reaction of OA by the $C_6F_5^-$ ligand, similar to the observed for AuAg ultrathin nanorods and nanowires,[18] we have also observed in the $^{13}C\{^1H\}$ NMR spectrum of washed Au CSs (**1**) that the OA ligands would interact with the surface of Au NPs forming the Au CSs through their carboxylic groups acting as capping ligand for the individual Au NPs and, also, for the Au CSs, since a clear shift upfield of the signal assigned to the carboxylic acid group is detected. However, the presence of sharp signals also agrees with a fast dynamic equilibrium between bound and free OA. The IR spectrum of OA and washed Au CSs (**1**) were recorded on KBr substrates (see ESI†). The most important observation is that oleate molecules are not formed at the surface of the nanoparticles. The typical absorption bands of OA are observed for a washed sample of Au CSs (**1**), for which only the capping OA would still remain interacting with the Au NPs surface.
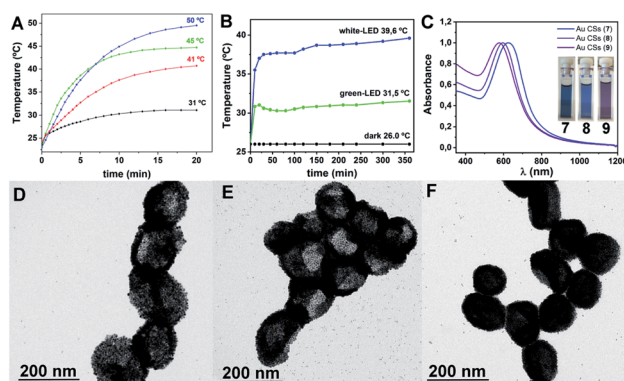

Fig. 6 Temperature increase of a 2.2 mM (red), 8.9 mM (green) and 22.2 mM (blue) ethanol solutions of Au CSs (**1**) and temperature increase of the free solvent (black) with time (A). Plasmonic-assisted temperature increase with time of the reaction mixture for the synthesis of Au CSs under white-LED light (blue), green-light (green) and under dark conditions (black) (B). Normalized UV/Vis spectra of Au CSs **7–9** in *n*-hexane (C). TEM image of Au CSs **7** (D), **8** (E) and **9** (F).

White-light induced photothermal heating and plasmonic assisted synthesis of Au CSs

The intense visible light plasmonic absorption of Au CSs (**1**) (max. 622 nm) arising from the plasmonic coupling of Au NPs, prompted us to study the white-light induced photothermal heating of the colloidosomes. This type of light harvesting has been less studied compared to NIR-light one and requires broadband optical absorbers able to harvest light over all the visible region.[25] The Au CSs reported here fulfil this requirement, displaying an absorption in most of the visible region, which strongly overlaps with the light from a white-LED source (max. 470; broad shoulder at 570 nm), leading to a strong light absorption and scattering by the Au CSs. A dispersion of Au CSs (**1**) (8.9 mM) in ethanol was exposed to one white-LED source (200 mW cm^{-2}) while the temperature of the solution was measured over time.

Fig. 6A depicts the photothermal heating of **1** that rose *ca.* 22 °C, up to 45 °C. We have also studied the influence of the Au CSs concentration on the photothermal heating property. We have observed that at lower concentration (2.22 mM) the photothermal heating decreases to 41 °C while at higher concentration (22.2 mM) it increases to 50 °C, showing an interesting potential for the design of photothermal heating devices. In order to take advantage of this white-light induced photothermal heating we tested the plasmonic-assisted synthesis[26] of Au CSs by substituting the thermal heating by photothermal heating, using a four-LED device. We carried out the synthesis of Au CSs in the same conditions as for Au CSs **1** in three different experiments, namely: (i) white-LED light irradiation; (ii) green-LED light irradiation (523 nm) and; (iii) dark conditions. We monitored the temperature over time and we observed that for the plasmonic-assisted synthesis with white light, after 30 min of reaction, the temperature reached 38 °C and this temperature was kept between 38–40 °C during the 6 h of reaction (Fig. 6B). When the monochromatic green light was employed, also after 30 min of reaction a stable temperature

value was reached but, in this case, only 31 °C were reached (see Fig. 6B). The results show that the use of white-light permits the synthesis of Au CSs (**7**), which are very similar in size (*ca.* 167 nm) and shape and show a very similar plasmonic absorption (626 nm) to that of Au CSs (**1**), obtained under thermal conditions. The use of green-LED light, although it assists the formation of Au CSs (**8**), they show a blue-shifted plasmonic absorption (596 nm) with a smaller size (*ca.* 147 nm), and they appear agglomerated and mixed with spherical Au NPs. Finally, in the dark, at RT, agglomerations of Au NPs into spherical shapes of *ca.* 118 nm (**9**) with an even more blue-shifted plasmonic absorption at 575 nm were obtained (see Fig. 6C). This white-light induced photothermal heating property makes these materials potentially useful for the design of broadband optical absorption materials at higher concentrations.[19,27]

Stimuli-responsive properties of Au CSs

To further show the ability of these Au CSs to switch their plasmonic properties, we also wanted to prove their dynamic nature in disassembly/reassembly experiments provoked by stimuli-responsive changes. For example, we have observed that the use of solvent as stimulus allows the disassembly/reassembly of freshly prepared compact Au CSs (**1**). Thus, when the reaction solvent *n*-hexane is evaporated and EtOH or THF is added, keeping the OA of the reaction mixture, a ruby-red solution corresponding to the structural disruption of the Au CSs into separated Au NPs is obtained. Then, upon evaporation of EtOH or THF and addition of *n*-hexane new spherical aggregates displaying a broad plasmonic absorption at 645 nm are obtained in a new aggregation process, leading to OA nanodroplet template-assisted aggregation of individual Au NPs. This reassembly leads to spherical shapes with a new and characteristic plasmonic coupling, red-shifted with respect to the one obtained for the Au CSs (**1**), and displaying a broader band with a tail in the NIR region (see Fig. 7). In the case of the nanostructures formed after the reassembly of Au CSs (**1**), the

HAADF-STEM analysis shows that these nanostructures consists of compact aggregates, instead of hollow Au CSs (see ESI†). A recent result by Park *et al.*[28] compares the morphology and plasmonic properties of hollow/porous Au nanoshells obtained through a laser-induced fabrication approach with crushed and flattened Au NPs aggregates. In a similar way to the disassembly–reassembly process described herein, the plasmon absorption of the hollow/porous Au nanoshells appears at *ca.* 780 nm whereas the Au NPs aggregates appears at *ca.* 830 nm as a broad band. DLS measurements (intensity distribution) of the disassembly/reassembly process confirm the TEM observations. Before disassembly a main population of *ca.* 112 nm size is obtained, which upon disassembly leads to three main populations of *ca.* 7, 35 and 175 nm. Taking into account that for DLS intensity distributions a very small amount of a larger aggregate species would have a large bias on the signal (intensity is proportional to diameter to the sixth power), we represented for the disassembly situation the DLS volume distribution, for which a main population of *ca.* 6 nm is observed. After reassembly, aggregates of *ca.* 410 nm are obtained, representing the aggregation of spherical shapes as in Fig. 7E (see ESI†).

The physical origin of the disassembly/reassembly process could be related to the presence of OA during the solvent exchange process and the different behaviour of OA in these solvents, which provides a high solubility and miscibility in EtOH or THF, but leads to formation of OA nanodroplets in low-polar *n*-hexane or toluene. It is important to note that when Au CSs are subjected to washing with ethanol and the excess of OA is eliminated, this disassembly/reassembly process does not take place, even if OA is added afterwards, showing the main role of OA in this process.

Interestingly, Au CSs may suffer a selective stimuli-responsive structural change that depends on the way that the tri-peptide glutathione (GSH) is added. Addition of 1 mL of a 50 mM solution of GSH in water in 10 × 100 μL portions to Au CSs (**1**) in EtOH allows the substitution of the OA by GSH, leading to significant changes in the size and the shape of the nanostructure going from Au CSs (**1**) of 179 ± 29 nm and Au NPs of 4.0 ± 1.5 nm size to Au CSs (**10**) of 164 ± 41 nm and Au NPs of 5.9 ± 1.4 nm size. Indeed, it can be observed that after the addition of GSH some of the smallest spherical nanoparticles appear displaced out of the colloidosomes (Fig. 8A). This is confirmed observing the size distribution of the spherical nanoparticles, which form the colloidosomes, going from an average of 4.0 nm in Au CSs (**1**) to 5.5 nm in Au CSs (**10**) (see ESI†) These morphology changes together with the important surface changes that take place when a carboxylic functional group (OA) is replaced with a thiol group (GSH), lead to an important optical response change with a red-shifting and broadening of the plasmon absorption band to 660 nm for Au CSs (**10**) (Fig. 8B). A very important result is that upon ligand exchange, Au CSs become hydrophilic, what opens the way for their use in aqueous systems. However, when compact Au CSs (**6**) are treated with 1 mL of a 50 mM solution of GSH in water in 20 × 50 μL portions, Au CSs are obtained but they start to disrupt and open their structures. Addition of GSH in 10 × 100 μL portions leads to almost disrupted CSs, whereas the addition of 1 mL of GSH at once gives rise to the complete opening of the CSs (Fig. 8C–F). This result is accompanied by a clear blue-shift of the plasmonic absorption from 622 nm for Au CSs (**6**) to 585, 570 and, finally to 530 nm, respectively (Fig. 8G). The possibility of OA–GSH ligand substitution by the better affinity of thiol groups to gold, keeping the CSs structure can be realized only if
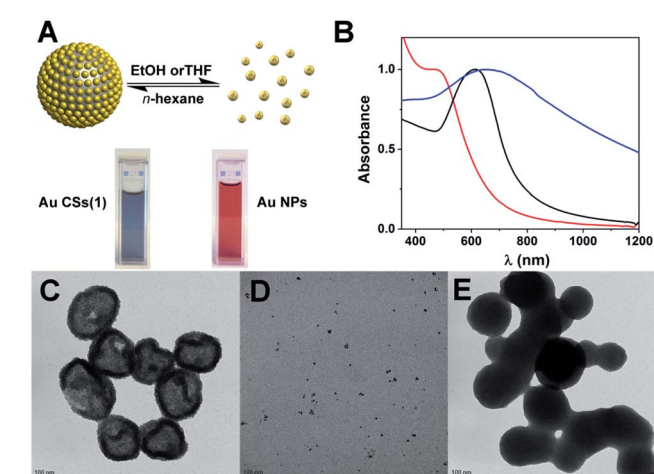

Fig. 7 Solvent-dependent disassembly/reassembly of Au CSs (**1**) (A) and corresponding UV/Vis spectra before disassembly with a maximum at 622 nm (black), after disassembly with a shoulder at *ca.* 500 nm (red) and reassembly into Au NP aggregates at 645 nm (blue) (B). TEM images of the disassembly/reassembly of Au CSs (**1**) (C–E).
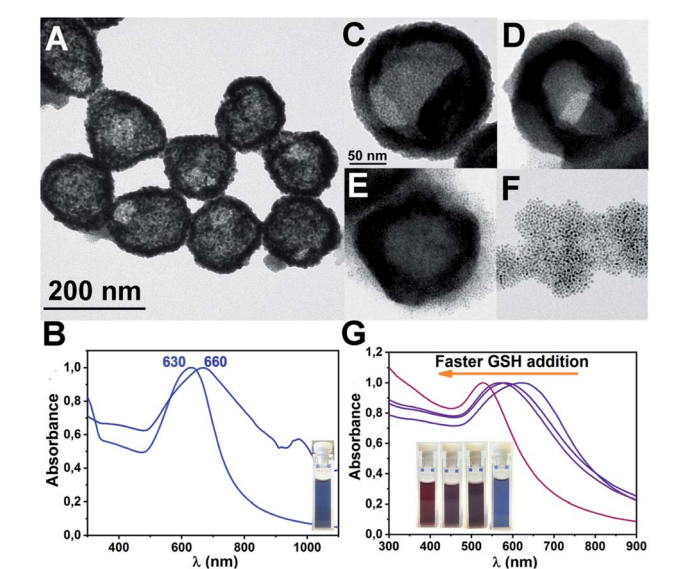

Fig. 8 TEM image of Au CSs (**10**) (A) and UV/Vis spectrum of Au CSs (**1**) and Au CSs (**10**) in ethanol after substitution of oleic acid by GSH (the absorption at *ca.* 950 nm corresponds to ethanol) (B). TEM images of Au CSs (**6**) in ethanol (C) and after addition 1 mL of a 50 mM solution of GSH in water in 20 × 50 μL portions (D); addition of GSH in 10 × 100 μL portions (E) or addition of 1 mL of GSH at once (F), showing the CSs structural disruption. UV/Vis spectra showing the plasmonic changes in C–F (G).

the OA capping ligands at the external part of the CSs are substituted; and a slow process by addition of small concentrations of GSH can do this. However, a faster GSH addition provokes the substitution of a larger amount of OA due to the higher local concentration of GSH at a given time, leading to the observed structural dissociation. This result opens the way for the use of these systems in drug release applications since GSH is a widely existing tri-peptide in cells.

Experimental

General

The compound $[Au(C_6F_5)(tht)]$ was synthesized by a standard procedure reported in the literature.[29] Oleic acid (OA) and triisopropylsilane (TIPS) were purchased from Sigma-Aldrich and used without any purification. All synthetic approaches were carried out in Ace pressure tubes, in oil bath at 60 °C, or at RT under LED-light irradiation. After 2 hours of reaction, the reaction mixtures were centrifuged, discarding the supernatant. Every experiment was repeated at least twice in order to ensure its reproducibility.

Instrumentation

The NMR spectra were recorded on a Bruker Avance 400 and ARX 300 spectrometers in d^8-toluene solutions. UV/Vis/NIR spectra were recorded with a Shimadzu UV-3600 UV-Vis-NIR spectrophotometer. Nanoparticle Tracking Analysis (NTA) was carried out with a Nanosight NS300 device from Malvern, equipped with a 45 mW laser working at $\lambda = 488$ nm. Video sequences were recorded via a high sensitivity sCMOS camera operating at 25 frames per second and evaluated via the NANOSIGHT NTA 2.0 Analytical Software Suite. DLS measurements were performed on a Brookhaven Instruments Corporation 90 PLUS particle size analyser on ethanol or n-hexane solutions to yield the size distributions by intensity. Samples for Transmission Electron Microscopy (TEM) were directly drop-casted from n-hexane or ethanol dispersions before centrifugation (2–3 drops) over carbon-coated Cu grids. TEM images were obtained with a JEOL JEM 2100 microscope. Scanning Transmission Electron Microscopy (STEM) measurements were performed in a Tecnai F30 (Thermofisher) at a working voltage of 300 kV. High Angle Annular Dark Field (HAADF) images were obtained with a Fischione detector. On the other hand, Energy Dispersive X-ray Spectra (EDS) were acquired with an EDAX detector. Point spectra and linescans were obtained in order to confirm the chemical composition and hollow structure of the colloidosomes. The light emitting diode system (LED) used for photothermal heating experiments and for plasmonic-assisted synthesis consisted of four, 10 W cool white LedEngin LZ4-00CW08 white light emitters or four 10 W 523 nm LedEngin LZ4-40G108 green emitters attached to a home-made water-cooled aluminium heat sink device.

Synthesis of Au CSs (1–3)

Complex $[Au(C_6F_5)(tht)]$ (10 mg, 0.022 mmol) (**1**); (5 mg, 0.011 mmol) (**2**) or (15 mg, 0.033 mmol) (**3**) was suspended in 2.5 mL

of n-hexane and then oleic acid (100 µL, 0.32 mmol) was added. The suspension was sonicated for 3 minutes in order to dissolve the gold complex and triisopropylsilane (150 µL, 0.73 mmol) was added. The reaction mixture was left without stirring in an Ace pressure tube inside an oil bath at 60 °C. After 2 hours, a blue solution was formed, and it was used for UV/Vis/NIR and TEM sampling.

The solid was separated from the solution by centrifugation discarding the supernatant. These blue Au CSs are soluble in EtOH, n-hexane or toluene, keeping its UV/Vis/NIR spectrum unaltered.

Synthesis of Au CSs (4–5)

To a n-hexane (2.5 mL) suspension of $[Au(C_6F_5)(tht)]$ (10 mg, 0.022 mmol), oleic acid was added (50 µL, 0.16 mmol (**4**) or 300 µL, 0.95 mmol (**5**)), and the mixture was sonicated for 3 minutes to dissolve the gold complex. After that, triisopropylsilane (150 µL, 0.73 mmol) was added and the mixture was left without stirring in an Ace pressure tube in oil bath at 60 °C for 2 hours, forming a blue solution. This blue solution was used for UV/Vis/NIR and TEM sampling.

The solid was separated from the solution by centrifugation discarding the supernatant. These blue Au CSs are soluble in EtOH, n-hexane or toluene, keeping its UV/Vis/NIR spectrum unaltered.

Synthesis of Au CSs (6)

A suspension of $[Au(C_6F_5)(tht)]$ (10 mg, 0.022 mmol) was prepared in 2.5 mL of n-hexane and then, oleic acid (100 µL, 0.32 mmol) was added. The mixture was sonicated for 3 minutes in order to dissolve $[Au(C_6F_5)(tht)]$, and triisopropylsilane (450 µL, 2.20 mmol) was added. The reaction mixture was left without stirring in Ace pressure tube in oil bath at 60 °C for 2 hours, forming a blue solution. This was used for UV/Vis/NIR and TEM sampling.

The solid was separated from the solution by centrifugation and discarding the supernatant. These blue Au CSs are soluble in EtOH, n-hexane or toluene, keeping its UV/Vis/NIR spectrum unaltered.

Synthesis of Au CSs (7–9)

To a n-hexane (2.5 mL) suspension of $[Au(C_6F_5)(tht)]$ (10 mg, 0.022 mmol), oleic acid was added (100 µL, 0.32 mmol). The mixture was sonicated for 3 minutes until the complete solution of $[Au(C_6F_5)(tht)]$ and triisopropylsilane (150 µL, 2.20 mmol) was added. The mixture, without stirring, was exposed to white (**7**) or green LED-light (**8**), or left under darkness conditions (**9**), for 6 hours, forming blue solutions. These solutions were used for UV/Vis/NIR and TEM sampling.

Synthesis of Au CSs (10)

The blue solid obtained by centrifugation of Au CSs (**1**) was dissolved in EtOH (2 mL) and 1 mL of L-glutathione (50 mM in water) was added in 10 × 100 µL portions under stirring. The blue solution remained unaltered and, after 5 minutes of

stirring, it was centrifuged, discarding the supernatant. This new blue Au-nanostructures are now soluble in water, keeping its UV/Vis/NIR spectrum unaltered.

Conclusions

In conclusion, we have developed a single-step method for the synthesis of sub-200 nm Au CSs of controlled diameter and surface, taking advantage of the formation of small Au NPs at the interface of oleic acid nanodroplets templates in *n*-hexane. These Au CSs display tuneable size and surface-dependent collective plasmonic properties arising from the coupling of the individual Au NP plasmons. In addition, these Au CSs display white-LED light induced photothermal heating that can be used, for example, for the plasmonic-assisted synthesis of the CSs. The Au CSs also display stimuli-responsive properties to solvent changes or to the addition of glutathione. We envision that these Au-based plasmonic nanostructures constitute an interesting model for the study of further plasmonic related properties such as photothermal heating, (photo)catalysis or drug release.

Conflicts of interest

There are no conflicts to declare.

Acknowledgements

Notes and references

1 M. A. Boles, M. Engel and D. V. Talapin, *Chem. Rev.*, 2016, **116**, 11220–11289.
2 B. A. Grzybowski, K. Fitzner, J. Paczesny and S. Granick, *Chem. Soc. Rev.*, 2017, **46**, 5647–5678.
3 A. Sánchez-Iglesias, N. Claes, D. M. Solís, J. M. Taboada, S. Bals, L. M. Liz-Marzán and M. Grzelczak, *Angew. Chem., Int. Ed.*, 2018, **57**, 3183–3186.
4 A. D. Dinsmore, M. F. Hsu, M. G. Nikolaides, M. Marquez, A. R. Bausch and D. A. Weitz, *Science*, 2002, **298**, 1006–1009.
5 K. L. Thompson, M. Williams and S. P. Armes, *J. Colloid Interface Sci.*, 2014, **447**, 217–228.
6 S. Shilpi, A. Jain, Y. Gupta and S. Jain, *Crit. Rev. Ther. Drug Carrier Syst.*, 2007, **24**, 361–391.
7 A. San Miguel and S. H. Behrens, *Soft Matter*, 2011, **7**, 1948–1956.
8 M. Liu, Q. Tian, Y. Li, B. You, A. Xu and Z. Deng, *Langmuir*, 2015, **31**, 4589–4592.
9 K. Larson-Smith and D. C. Pozzo, *Langmuir*, 2012, **28**, 11725–11732.
10 M. Dhiman, A. Maity, A. Das, R. Belgamwar, B. Chalke, Y. Lee, K. Sim, J. M. Nam and V. Polshettiwar, *Chem. Sci.*, 2019, **10**, 6594–6603.
11 L. Zhang, Q. Fan, X. Sha, P. Zhong, J. Zhang, Y. Yin and C. Gao, *Chem. Sci.*, 2017, **8**, 6103–6110.
12 D. Liu, F. Zhou, C. Li, T. Zhang, H. Zhang, W. Cai and Y. Li, *Angew. Chem.*, 2015, **127**, 9732–9736.
13 F. Sciortino, G. Casterou, P. A. Eliat, M. B. Troadec, C. Gaillard, S. Chevance, M. L. Kahn and F. Gauffre, *ChemNanoMat*, 2016, **2**, 796–799.
14 F. Sciortino, M. Thivolle, M. L. Kahn, C. Gaillard, S. Chevance and F. Gauffre, *Soft Matter*, 2017, **13**, 4393–4400.
15 J. García-Barrasa, J. M. López-de-Luzuriaga, M. Monge, K. Soulantica and G. Viau, *J. Nanopart. Res.*, 2011, **13**, 791–801.
16 J. Crespo, A. Falqui, J. Garcia-Barrasa, J. M. Lopez-de-Luzuriaga, M. Monge, M. E. Olmos, M. Rodriguez-Castillo, M. Sestu and K. Soulantica, *J. Mater. Chem. C*, 2014, **2**, 2975–2984.
17 J. Crespo, A. Ibarra, J. M. López-de-Luzuriaga, M. Monge and M. E. Olmos, *Eur. J. Inorg. Chem.*, 2014, **2014**, 2383–2388.
18 J. Crespo, J. M. López-de-Luzuriaga, M. Monge, M. Elena Olmos, M. Rodríguez-Castillo, B. Cormary, K. Soulantica, M. Sestu and A. Falqui, *Chem. Commun.*, 2015, **51**, 16691–16694.
19 S. J. Oldenburg, R. D. Averitt, S. L. Westcott and N. J. Halas, *Chem. Phys. Lett.*, 1998, **288**, 243–247.
20 Y. Guan, Z. Xue, J. Liang, Z. Huang and W. Yang, *Colloids Surf., A*, 2016, **502**, 6–12.
21 Y. C. Wang, É. Rhéaume, F. Lesage and A. Kakkar, *Molecules*, 2018, **23**, 1–28.
22 N. J. Halas, S. Lal, W. Chang, S. Link and P. Nordlander, *Chem. Rev.*, 2011, **111**, 3913–3961.
23 P. K. Jain, W. Huang and M. A. El-sayed, *Nano Lett.*, 2007, **7**, 2080–2088.
24 H. Lange, B. H. Juárez, A. Carl, M. Richter, N. G. Bastús, H. Weller, C. Thomsen, R. Von Klitzing and A. Knorr, *Langmuir*, 2012, **28**, 8862–8866.
25 S. H. Tsao, D. Wan, Y. S. Lai, H. M. Chang, C. C. Yu, K. Te Lin and H. L. Chen, *ACS Nano*, 2015, **9**, 12045–12059.
26 R. Kamarudheen, G. W. Castellanos, L. P. J. Kamp, H. J. H. Clercx and A. Baldi, *ACS Nano*, 2018, **12**, 8447–8455.
27 H. Zhang, L. Feng, Y. Liang and T. Xu, *Nanoscale*, 2019, **11**, 437–443.
28 T. H. Park and D. J. Jang, *Nanoscale*, 2018, **10**, 20108–20112.
29 R. Usón, A. Laguna and J. Vicente, *J. Chem. Soc., Chem. Commun.*, 1976, 353–354.